J Biomol NMR (2011) 50:347–355
DOI 10.1007/s10858-011-9520-6

ARTICLE

# Quantifying millisecond time-scale exchange in proteins by CPMG relaxation dispersion NMR spectroscopy of side-chain carbonyl groups

**Alexandar L. Hansen · Lewis E. Kay**

Received: 20 April 2011 / Accepted: 19 May 2011 / Published online: 18 June 2011


**Abstract** A new pulse sequence is presented for the measurement of relaxation dispersion profiles quantifying millisecond time-scale exchange dynamics of side-chain carbonyl groups in uniformly $^{13}C$ labeled proteins. The methodology has been tested using the 87-residue colicin E7 immunity protein, Im7, which is known to fold via a partially structured low populated intermediate that interconverts with the folded, ground state on the millisecond time-scale. Comparison of exchange parameters extracted for this folding 'reaction' using the present methodology with those obtained from more 'traditional' $^{15}N$ and backbone carbonyl probes establishes the utility of the approach. The extracted excited state side-chain carbonyl chemical shifts indicate that the Asx/Glx side-chains are predominantly unstructured in the Im7 folding intermediate. However, several crucial salt-bridges that exist in the native structure appear to be already formed in the excited state, either in part or in full. This information, in concert with that obtained from existing backbone and side-chain methyl relaxation dispersion experiments, will ultimately facilitate a detailed description of the structure of the Im7 folding intermediate.

**Keywords** CPMG · Relaxation dispersion · Im7 · Side-chain carbonyl groups · Excited protein states

**Electronic supplementary material** The online version of this article (doi:10.1007/s10858-011-9520-6) contains supplementary material, which is available to authorized users.

A. L. Hansen · L. E. Kay (✉)
Departments of Molecular Genetics, Biochemistry and Chemistry, The University of Toronto, Toronto, ON M5S 1A8, Canada
e-mail: kay@pound.med.utoronto.ca

L. E. Kay
Program in Molecular Structure and Function, Hospital for Sick Children, 555 University Avenue, Toronto, ON M5G 1X8, Canada

## Introduction

Proteins are not static entities, often exchanging between different conformations that are important for biological function (Karplus and Kuriyan 2005). As such, knowledge of the structural and functional properties of these different conformational states is critical. Uncovering these details, however, is often thwarted by the fact that many of the interconverting states are populated only transiently and at low levels so that they are invisible to 'traditional' structural biology techniques (Baldwin and Kay 2009; Boehr et al. 2006; Fraser et al. 2009). Further, in most cases it is not possible to trap these conformations in a form where they can be studied directly. Thus, little detailed structural and motional data is presently available for these rare (excited) conformational states. The situation is changing, however, with the development of Carr-Purcell-Meiboom-Gill (CPMG) relaxation dispersion NMR methods that are sensitive to exchange processes occurring in the millisecond (ms) time window (Hansen et al. 2008b; Palmer et al. 2001). So long as the exchange kinetics are in the slow to intermediate regime and fractional populations of excited states are on the order of 0.5% or larger, CPMG relaxation dispersion profiles can be fitted to extract exchange rates and relative populations of interconverting states and, most importantly, absolute values of differences in chemical shifts between ground ($\varpi_G$, ppm) and excited ($\varpi_E$) conformers (Korzhnev et al. 2004; Palmer et al. 2001). Values of $|\Delta\varpi|$ ($\Delta\varpi = \varpi_E - \varpi_G$) can subsequently be recast in terms of the chemical shifts of the excited state, $\varpi_E = \Delta\varpi + \varpi_G$, so long as the sign of $\Delta\varpi$ is known from

separate experiments (Auer et al. 2009; Bouvignies et al. 2010; Skrynnikov et al. 2002).

Relaxation dispersion methods are now available for measuring $^{15}N$ (Hansen et al. 2008a; Loria et al. 1999; Tollinger et al. 2001), $^{1}H^{N}$ (Ishima and Torchia 2003; Orekhov et al. 2004), $^{13}CO$ (Ishima et al. 2004; Lundstrom et al. 2008), $^{13}C^{\alpha}$ (Hansen et al. 2008c) and $^{1}H^{\alpha}$ (Lundstrom et al. 2009) backbone chemical shifts in excited protein states. Such chemical shifts serve as powerful restraints for structure determination of these elusive conformers, especially when used in concert with computational database approaches such as CS-Rosetta (Shen et al. 2009), Cheshire (Cavalli et al. 2007) or CS23D (Wishart et al. 2008). As an example, our laboratory has recently published the structure of a low populated folding intermediate based on chemical shifts and orientational restraints that were obtained from a variety of different relaxation dispersion approaches (Korzhnev et al. 2010).

With robust experiments for measurement of backbone chemical shifts in excited protein states now available, at least for applications to small proteins, we have become interested in developing approaches for using side-chain probes in studies of low populated conformers. In this regard, experiments for exploiting methyl groups have been in use for over a decade (Skrynnikov et al. 2001), with improvements that increase their sensitivity published more recently (Lundstrom et al. 2007). Pulse schemes have also been developed for measuring $^{15}N$ CPMG dispersion profiles of side-chain $NH_2$ groups of Asn/Gln (Mulder et al. 2001) and of $NH_3^+$ moieties of Lys (Esadze et al. 2011). Another attractive probe is the side-chain carbonyl group of Asx/Glx residues since extracted $\Delta\varpi$ values may reflect changes in electrostatic interactions brought about by structural rearrangements in the exchanging states that would be of importance to quantify. Asx/Glx residues comprise slightly more than 20% of the amino acids in a 'typical' bacterial protein (Gerstein 1997), encouraging the development of CPMG dispersion experiments that are focused on their side-chains. Herein we present a pulse scheme for simultaneous measurement of Asx/Glx side-chain carbonyl CPMG dispersion profiles in proteins and apply the methodology to the colicin E7 binding immunity protein, Im7. This small (87 amino acid) four helical bundle protein (Capaldi et al. 2002, 2001) has been shown previously to fold via an on-pathway intermediate that has been characterized by a variety of biophysical techniques. Most important for the present application is the significant number of Asx (13) and Glx (13) residues (30% of amino acids), suggesting that side-chain carbonyl moieties will be an excellent probe of the excited state folding intermediate in this system.

## Materials and methods

### Protein sample preparation

Isotopically enriched samples of the wild-type Im7 protein were expressed using a pTrc99-A (Pharmacia) based expression vector (Le Duff et al. 2006) with BL21-CodonPlus(DE3)-RIL competent cells (Stratagene). The cells were grown in M9 minimal media using 1 g/L of $^{15}NH_4Cl$ and 3 g/L of U-$^{1}H$,$^{13}C$-glucose as the sole nitrogen and carbon sources, respectively, using chloramphenicol and carbenicillin antibiotics. The cells were grown at 37°C to an OD of 0.8–1.0 before induction with 1 mM IPTG and protein expression was allowed to continue overnight at room temperature with a final OD between 2.5 and 3.0. Cells were pelleted at 6,000 g for 20 min and resuspended in ~25 mL of lysis buffer (50 mM Tris pH 7.5, 50 mM KCl, 1 mM EDTA, DNase I, lysozyme, and a protease inhibitor cocktail tablet, EDTA-free (Roche)) before storing at −20°C overnight. Subsequently the cells were thawed, lysed using a homogenizer and pelleted at 30,000 g for 20 min. Im7 was purified from the supernatant by anion exchange chromatography (GE Healthcare HiTrap Q XL) followed by buffer exchange into 50 mM potassium phosphate pH 7.0, 150 mM KCl and gel filtration (GE Healthcare Hiload 10/60 Superdex 75 pg). The collected fractions were concentrated and exchanged into NMR buffer (50 mM potassium phosphate, pH 6.6, 0.02% azide) that was either 100% $D_2O$ or 95% $H_2O$/5% $D_2O$. Samples used in the present studies were 1.4 mM in protein.

### NMR spectroscopy

Side-chain carbonyl group relaxation dispersion data sets were recorded at static magnetic fields of 11.7 and 18.8 T using the pulse scheme of Fig. 1. Notably, a doubly band-selective constant adiabaticity WURST-8 decoupling scheme (Kupce and Freeman 1996; Kupce and Wagner 1996) was used to eliminate polarization transfer to Asx $C^{\alpha}$ or Glx $C^{\beta}$ nuclei while still allowing simultaneous collection of Asx $C^{\gamma}$ and Glx $C^{\delta}$ CPMG dispersion data. Data sets (25°C) were obtained with 16 (18) $\nu_{CPMG}$ values ($T_{relax} = 40$ ms) ranging from 25 to 900 Hz (25–1,100 Hz) at 11.7 (18.8) T, including three $\nu_{CPMG}$ repetitions for error analysis. Each 2D spectrum (11.7 T) was recorded with (90, 512) complex points in ($t_1$, $t_2$), corresponding to acquisition times of (75 ms, 64 ms), and a delay between scans of 2.0 s, for a net measurement time of 50 min. Data sets obtained at 18.8 T comprised (100, 512) complex points, acquisition times of (52 ms, 64 ms), and were recorded with a relaxation delay of 2.0 s and an acquisition time of 58 min/spectrum. Similar acquisition parameters were obtained for data

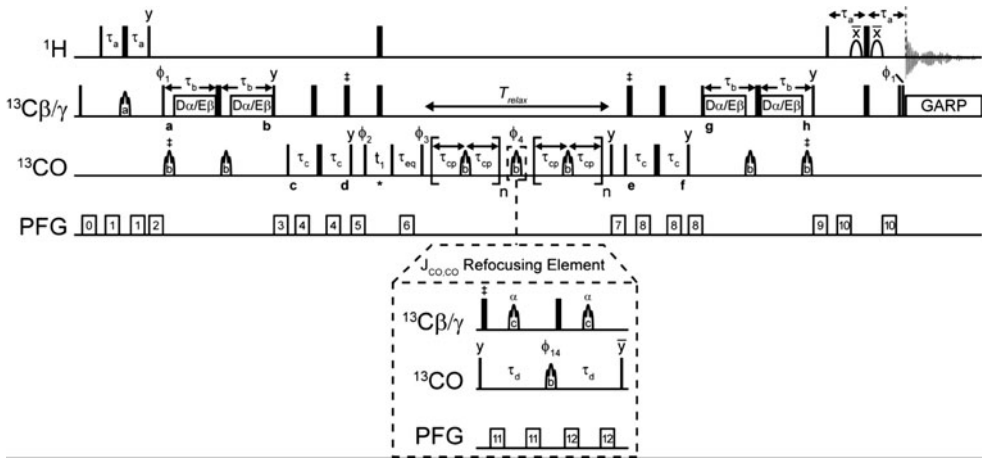


**Fig. 1** Pulse sequence for recording Asx/Glx side-chain carbonyl CPMG relaxation dispersion profiles in uniformly $^{13}$C-labeled proteins. The $^{1}$H carrier is centered on the water signal while the $^{13}$C transmitter is positioned at either 38.5 ppm (aliphatic $^{13}C^{\beta/\gamma}$) or 181 ppm ($^{13}$CO), with the exception of the shaped pulses (indicated with '*c*') in the $J_{CO,CO}$ refocusing element that are selective for the $^{13}C^{\alpha}$ region of the spectrum and centered at 56 ppm. *Narrow* and *wide vertical bars* denote 90° and 180° rectangular pulses, respectively, of phase *x* unless indicated otherwise. $^{1}$H and $^{15}$N pulses are delivered with the maximum power available, while $^{13}$C rectangular pulses are applied with a power of $\Delta\Omega/\sqrt{15}$ (90°) or $\Delta\Omega/\sqrt{3}$ (180°) where $\Delta\Omega$ equals 142.5 ppm. Shaped pulses '*a*' and '*c*' are of the REBURP variety (Geen and Freeman 1991), with durations of 2.4 (1.5) ms at 11.7 (18.8 T). Shaped pulses labeled '*b*' are optimized for refocusing the carbonyl region of the spectrum while minimally perturbing aliphatic $^{13}$C spins (Lundstrom et al. 2008) and are applied with lengths of 450 (11.7 T) or 380 (18.8 T) μs. Shaped pulses on the $^{1}$H channel are water selective 90° pulses (used only for samples in $H_2O$ solvent) and have a length of ~1.4 ms. The *square blocks* labeled Dα/Eβ are band-selective constant adiabaticity WURST-8 decoupling schemes to eliminate polarization transfer to Asx $C^{\alpha}$ or Glx $C^{\beta}$ nuclei (Kupce and Freeman 1996; Kupce and Wagner 1996). The decoupling elements are centered at 55.0 ($C^{\alpha}$) and 28.25 ($C^{\beta}$) ppm, with bandwidths of 10.0 and 4.5 ppm, respectively, and are applied with maximum $B_1$ fields of 0.5 (0.6) kHz at 11.7 (18.8 T). The (*asterisk*) in the center of the $t_1$ evolution period indicates the position of a single $^{15}$N 180° pulse centered at 119 ppm to refocus evolution from side-chain $^{1}J_{C\gamma N\delta}$ and $^{1}J_{C\delta N\varepsilon}$ couplings. (*Double-daggers*) are used to indicate Bloch-Siegert compensation pulses (Vuister and Bax 1992). Delay times are $\tau_a = 1.85$ ms $\approx 1/(4J_{CH})$, $\tau_b = 4.9$ ms $\approx 1/(4J_{CCO})$, $\tau_c = 4.9$ ms $\approx 1/(4J_{CCO})$, $\tau_d = 9.8$ ms $\approx 1/(2J_{CCO})$, $\tau_{eq} = 3$ ms $\geq (2-3)/k_{ex}$. The value $T_{relax}$ (= $4n\tau_{cp}$) is chosen such that approximately 1/2 of the signal has decayed relative to $n = 0$ (30–40 ms for the applications considered here). When the refocusing element is (is not) used *n* can be any (*an even*) integer. The phase cycling used is $\phi_1 = x,-x$, $\phi_2 = 2(x),2(-x)$, $\phi_3 = 4(y),4(-y)$, $\phi_4 = y,-y$, $\phi_{14} = x,-x$, $\phi_{rec} = x,-x,-x,x,-x,x,x,-x$. Quadrature detection is obtained by incrementing $\phi_2$ and $\phi_{rec}$ according to the TPPI-States format (Marion et al. 1989). Gradient strengths in G/cm (lengths in ms) are: 0 = 8 (0.5), 1 = 10 (0.25), 2 = 50 (1.0), 3 = 16 (0.5), 4 = 16 (0.25), 5 = 20 (0.35), 6 = 20 (0.7), 7 = 12 (0.4), 8 = 12 (0.2), 9 = 28 (0.3), 10 = 24 (0.2), 11 = 6 (0.3), 12 = 13 (0.4). The pulse scheme can also be used to record backbone carbonyl CPMG relaxation dispersion profiles. $^{13}C^{\beta/\gamma}$ and $^{13}$CO carriers are set to 56 ppm and 176 ppm, respectively, and $\Delta\Omega = 120$ ppm. The decoupling elements between *a*, *b* and *g*, *h* are centered at 27.5 ppm with a 25 ppm bandwidth and with maximum $B_1$ field of 0.4 (0.5) kHz at 11.7 (18.8) T

recorded at 10°C but with $T_{relax} = 30$ ms. In addition to the side-chain carbonyl experiments backbone $^{15}$N and $^{13}$CO relaxation dispersion profiles were recorded using pulse schemes and acquisition parameters as described previously (Hansen et al. 2008c).

NMR data were processed and analyzed using the nmrPipe suite of programs (Delaglio et al. 1995) and Sparky (Goddard and Kneller) with peak volumes extracted using the program FuDa (http://pound.med.utoronto.ca/software.html). CPMG dispersion profiles were fit to a two-site exchange model, $A \underset{k_{BA}}{\overset{k_{AB}}{\longleftrightarrow}} B$, as described previously (Hansen et al. 2008c) using in-house written software, CATIA (http://pound.med.utoronto.ca/software.html). While the Im7 folding mechanism is known to be three-state (Whittaker et al. 2007), experimental conditions in our dispersion studies have been chosen to minimize the influence of the unfolded state such that its population cannot be detected. This is rigorously assessed in terms of the quality of fits and the uniformity of per-residue exchange parameters across the protein, enabling extraction of accurate exchange parameters and chemical shifts from data analysis involving the simplest of exchange models.

To obtain accurate excited state chemical shifts, dispersion profiles were first fitted on a per-residue and per-nucleus basis to extract $k_{ex} = k_{AB} + k_{BA}$, the population of the minor state, $p_B$, $|\Delta\varpi|$ and $R_{2,\infty}$, the intrinsic transverse relaxation rate in the absence of exchange. Those residues with $|\Delta\omega|/k_{ex} > 0.5$ (at both 11.7 and 18.8 T; $\Delta\omega$ in rad/s) and where $R_{ex} = R_2^{eff}(\nu_{CPMG} \rightarrow 0) - R_2^{eff}(\nu_{CPMG} \rightarrow \infty) \approx \frac{p_a p_b k_{ex} \Delta\omega^2}{p_a \Delta\omega^2 + k_{ex}^2}$ (Ishima and Torchia 1999; Millet et al. 2000) is greater than $0.2R_{2,\infty}$ were retained for global analysis (all data fitted together) to obtain the 'best' ($k_{ex}$, $p_B$) parameters. Overall, 12 (8) side-chain carbonyl dispersions were used to define the global parameters from the data recorded

at 25°C, $D_2O$ (10°C, 95% $H_2O$/5% $D_2O$). Using the optimal values for ($k_{ex}$, $p_B$) every dispersion profile was then fitted to extract $|\Delta\varpi|$. Errors in shift differences were calculated as the standard deviation of values extracted from fits of 1,000 bootstrap simulations (Press et al. 1988) of each dispersion profile. Inspection of these distributions showed them to be Gaussian. Values of $|\Delta\varpi|$ from the bootstrap simulations that were less than 0.01 ppm or greater than 5 ppm were excluded as they indicate poor fits of the simulated side-chain carbonyl dispersion data that would skew the error estimate.

## Results and discussion

Figure 1 illustrates the pulse scheme that has been developed for measurement of $^{13}C$ CPMG dispersion profiles from Asx/Glx side-chain carbonyl groups in U-[$^{13}C$]-labeled proteins. The similarity of $^{13}C^{\beta}/^{13}C^{\gamma}$ chemical shifts for Asx/Glx, as well as the corresponding $^{13}C^{\gamma}/^{13}C^{\delta}$ shifts for these residues, is exploited to record dispersion profiles for all four amino acids (Asp, Asn, Glu, Gln) simultaneously using a pulse scheme that is similar to previously developed HCCO sequences (Kay 1993). Neglecting pulse imperfections and relaxation and highlighting only the magnetization components that contribute to observable signal, the transfer pathway can be summarized as follows:

$$\begin{aligned} H^j_{TR} \xrightarrow{J_{HC}} 2H^j_Z C^j_{TR} \xrightarrow{J_{CjCO}} 4H_Z C^j_Z CO^k_{TR} \xrightarrow{J_{CjCO}} 2H_Z CO^k_{TR}(t_1, CPMG) \\ \xrightarrow{J_{CjCO}} 4H_Z C^j_Z CO^k_{TR} \xrightarrow{J_{CjCO}} 2H^j_Z C^j_{TR} \xrightarrow{J_{HC}} H^j_{TR}(t_2) \end{aligned} \quad (1)$$

In (1) $X_{TR}$ is transverse magnetization of spin $X$ ($^1H^j$, $^{13}C^j$ or side-chain $^{13}CO^k$), $j = \beta$ ($\gamma$), $k = \gamma$ ($\delta$) for Asx (Glx) and the arrows denote the relevant transfer steps that proceed via the scalar couplings indicated. Despite the fact that the sequence consists of simple transfer elements it is nevertheless worth pointing out the essential features that are critical to the robustness of the methodology. First, the transfer of magnetization is unidirectional, that is from $^{13}C^{\beta} \rightarrow {}^{13}C^{\gamma}$ (Asx) or $^{13}C^{\gamma} \rightarrow {}^{13}C^{\delta}$ (Glx). This is achieved through the application of band selective decoupling (Kupce and Wagner 1996) of $^{13}C^{\alpha}$ (Asx) and $^{13}C^{\beta}$ (Glx) spins between points $a$, $b$ and $g$, $h$ (see legend to Fig. 1) so that only the $^{13}C^{\beta}$–$^{13}C^{\gamma}$ (Asx) or $^{13}C^{\gamma}$–$^{13}C^{\delta}$ (Glx) couplings are active. In the case of the Im7 system considered here this decoupling scheme increases the sensitivity of the experiment twofold. Second, we have found it necessary to refocus side-chain $^{13}CO$ magnetization that is anti-phase with respect to the directly coupled $^{13}C$ spin prior to the CPMG element (between points $c$, $d$ of Fig. 1). Failure to do so results in significant artifacts in dispersion spectra, despite the fact that the CO refocusing pulses applied during the CPMG interval (labeled 'b' in Fig. 1) are selective for this region of the spectrum and simulations that include both the carbonyl and adjacent carbon spin indicate that the aliphatic carbon should not be affected by the pulses. The origin of the problem is not clear at present. Third, the central pulse in the CPMG element, applied with a phase orthogonal ($\phi_4$) to the remaining refocusing pulses, ensures that spurious magnetization created due to pulse imperfections in the first half of the CPMG interval is refocused by the end of this duration (Hansen et al. 2008a; Vallurupalli et al. 2007). Finally, for applications involving Asx residues we have modified the main sequence of Fig. 1 by including a '$J_{CO,CO}$ refocusing element' in the middle of the standard CPMG scheme. As described previously in some detail this scheme refocuses evolution due to three-bond scalar couplings connecting the side-chain carbonyl and backbone carbonyl carbons that can occur during the CPMG relaxation element (Lundstrom et al. 2008). Such evolution can lead to significant artifacts in the resultant dispersion profiles (Ishima et al. 2004; Lundstrom et al. 2008; Mulder and Akke 2003), as illustrated below for Im7. Additional couplings involving the side-chain carbonyl and aliphatic spins are refocused efficiently by the band selective pulses of the CPMG element and are not a concern in the present application.

It is worth indicating, however, that in the design of our pulse scheme we have not compensated for the differences in relaxation of in-phase and anti-phase components of $^{13}CO$ magnetization that evolve during the CPMG period (Loria et al. 1999). For the $T_{relax}$ and $\nu_{CPMG}$ values used in our experiments such effects are expected to be small and this has been verified through simulations that include experimentally measured estimates for the differential relaxation rates. We have also exploited the pH dependence of the population of the Im7 excited state to rigorously test that this is in fact the case. At pH 8.0 the excited state population is significantly reduced in comparison to pH 6.6 (where the majority of our experiments are conducted) so that flat dispersion curves would be anticipated for many of the residues in the absence of artifacts. For the majority of dispersion profiles we observe a small but systematic increase in $R_2^{eff}$(25 Hz) relative to the remaining relaxation rates, $R_2^{eff}(\nu_{CPMG})$, with $R_2^{eff}$(25 Hz) − $R_2^{eff}(\infty)$ $\sim 1.4 \pm 0.3$ s$^{-1}$ (25°C, 11.7 T) that results from scalar coupled evolution of CO magnetization with the directly attached $^{13}C^{\beta}$ (Asp) or $^{13}C^{\gamma}$ (Glu) spin. Such increases are consistent with measured Asx/Glx $^{13}C^{\beta/\gamma}$ $R_1$ values of $\sim 4$ s$^{-1}$ for Im7 (that approximates the difference in relaxation rates between in-phase $CO^k_{TR}$ and anti-phase $2C^j_Z CO^k_{TR}$ magnetization). Values of $R_2^{eff}$(50 Hz) − $R_2^{eff}(\infty)$ are on the order of $0.7 \pm 0.2$ s$^{-1}$, on average, while

$R_2^{eff}(75\ \text{Hz}) - R_2^{eff}(\infty) \sim 0.4 \pm 0.3\ \text{s}^{-1}$, so that differential relaxation influences primarily only the first point in each curve. Differences in in-phase/anti-phase relaxation rates will decrease as the measurement field strength and molecular size increase since for a rigid $^{13}$C spin with relaxation dominated by $^{1}$H-$^{13}$C dipolar interactions, $R_1$ rates scale as $1/(\omega^2\tau_C)$ in the macromolecular limit, where $\omega$ is the resonance frequency and $\tau_C$ is the overall tumbling time. These effects will also decrease as the duration of the CPMG relaxation element ($T_{relax}$) becomes smaller, that will be necessary for applications involving medium sized proteins. Artifacts of this sort are thus not expected to introduce significant errors into extracted exchange parameters or $|\Delta\varpi|$ values. Indeed, that this is the case is shown below where very similar ($k_{ex}$, $p_B$) values are derived from independent fits of side-chain $^{13}$CO and backbone $^{15}$N dispersion profiles recorded on the same sample.

The 2D $^{13}C^{\gamma/\delta}$-$^{1}H^{\beta/\gamma}$ correlation map of U-[$^{13}$C] Im7 recorded with the scheme of Fig. 1 ($T_{relax} = 0$), 25°C, 18.8 T, is shown in Fig. 2. Correlations for Asn and Glu fall in distinct regions of the spectrum and although resonance positions for Asp and Gln are more similar, in the case of the small Im7 protein all of the expected correlations are well resolved and can be quantified in CPMG dispersion experiments. Representative examples of dispersion profiles, $R_2^{eff}$ versus $\nu_{CPMG} = 1/(4\tau_{CP})$, where $2\tau_{CP}$ is the time between centers of successive refocusing pulses, are shown in Fig. 3. Data (circles) are recorded over a range of $\nu_{CPMG}$ values between 25 and approximately 1 kHz at static magnetic field strengths of 11.7 T (red) and 18.8 T (blue)

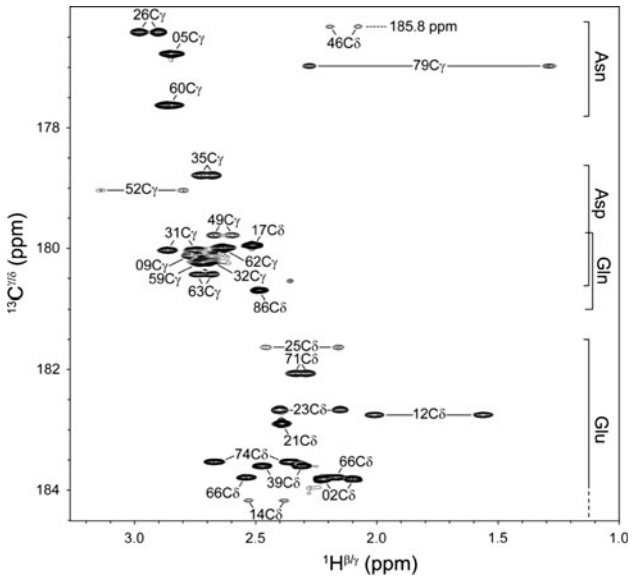


**Fig. 2** 2D $^{13}C^{\gamma/\delta}$-$^{1}H^{\beta/\gamma}$ correlation map of U-[$^{13}$C] Im7 recorded with the scheme of Fig. 1 ($T_{relax} = 0$), 25°C, pH 6.6, $D_2O$ solvent, 18.8 T. Assignments were obtained from a modified (HB)CBCACO(CA)HA triple-resonance experiment (Kay 1993)

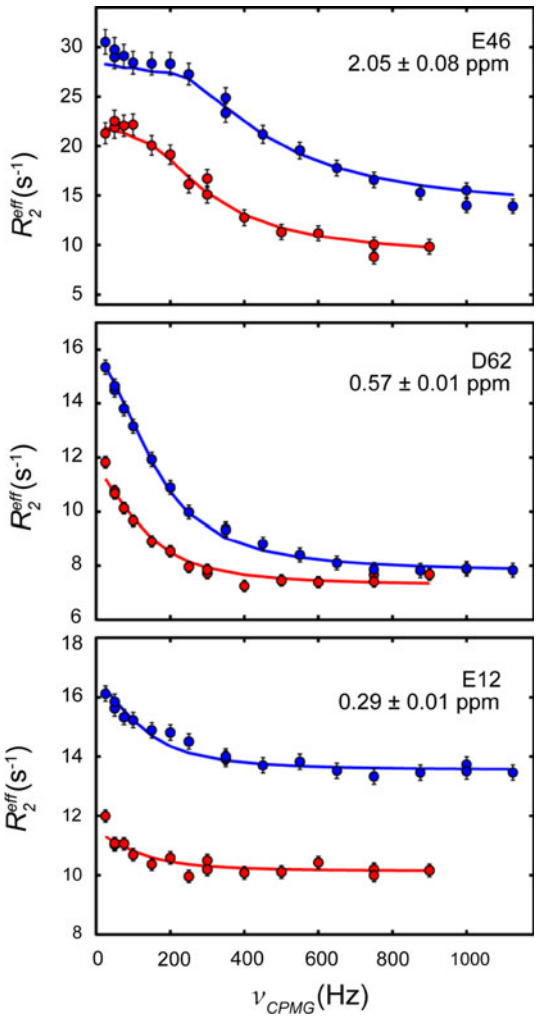


**Fig. 3** Representative side-chain $^{13}$CO CPMG relaxation dispersion curves measured on Im7 at 25°C, pH 6.6, $D_2O$ without the $J_{CO,CO}$ refocusing element. *Solid lines* indicate the best-fit of the data (*circles*) to a global two-site exchange model. Numbers in *insets* indicate fitted $|\Delta\varpi|$ values for each residue. *Red* and *blue* data points correspond to experiments recorded at 11.7 and 18.8 T, respectively. $^{3}J_{CO,CO}$ for Asp 62 is <1 Hz since the $C^{\gamma}$—backbone CO torsion angle for this residue is approximately 50° (Dennis et al. 1998)

using the pulse scheme of Fig. 1 in the absence of $J_{CO,CO}$ refocusing. The resultant dispersion profiles were fitted simultaneously to a model of two-site exchange with $k_{ex} = 737 \pm 22\ \text{s}^{-1}$ and a population of the minor state, $p_B$, of 2.07 ± 0.06%, 25°C, pH 6.6, 100% $D_2O$ (solid lines in Fig. 3). Extracted values of $|\Delta\varpi|$ are listed in the upper right hand corners of the panels of Fig. 3; random errors in shift differences are on the order of 2–4%, even for the weakest resonances, such as Glu 46 (Fig. 2, top). As a means of cross-validation we have used the scheme of Fig. 1 to record dispersion profiles of the backbone carbonyl carbons of Im7 (see figure legend) and the exchange parameters so obtained, ($k_{ex}$, $p_B$) = (721 ± 24 $\text{s}^{-1}$, 2.13 ± 0.05%), are in excellent agreement with the

corresponding parameters fitted from the side-chain data, providing confidence in the methodology. Finally, it is worth noting that when the backbone and side-chain CO dispersion data were fitted simultaneously to a two-site exchange model the global $\chi^2_{red}$ value increased by only approximately 10% relative to the corresponding value obtained from summing over $\chi^2$ values generated from per-residue fits, in strong support of the assumption of a two-state exchange mechanism.

The dispersion profiles of the side-chain carbonyl of Asp 62 in Fig. 3 were measured without the $J_{CO,CO}$ refocusing element of Fig. 1. From the X-ray structure of the Im7 protein (Chak et al. 1996; Dennis et al. 1998) the Asp 62 $C^{\gamma}$ and backbone CO carbons are gauche with respect to each other (dihedral angle of 50°) so that a small three-bond scalar coupling, $J_{CO,CO}$, is predicted for this residue (~0.5 Hz, Hu and Bax 1996). Artifacts in dispersion profiles due to evolution from $^3J_{CO,CO}$ would thus not be expected and are not observed in this case. By contrast, Asp 49 and Asn 26 are predicted to have large couplings (trans $C^{\gamma}$—backbone CO torsion angles corresponding to couplings of ~4 Hz, Hu and Bax 1996) so that significant distortions to the $R_2^{eff}(\nu_{CPMG})$ curves are anticipated in the absence of the refocusing element. Figure 4 shows that this is indeed the case, in particular for Asp 49, and that further, the refocusing element is effective at removing net evolution from these three-bond couplings.

Figure 5a presents a correlation plot of $|\Delta\varpi|$ values for Glx residues measured using the pulse scheme of Fig. 1 with (*Y*-axis) and without (*X*-axis) the $J_{CO,CO}$ refocusing element. As expected an excellent correlation is obtained since the band selective pulses refocus evolution from all $^{13}C$-$^{13}C$ homonuclear couplings during the CPMG element with the exception of $^4J_{CO,CO}$ that is negligibly small. A refocusing element is thus not needed. By contrast, the corresponding agreement is less good for Asx residues, Fig. 5b, since trans $C^{\gamma}$—backbone CO torsion angles are calculated from the X-ray structure (Chak et al. 1996; Dennis et al. 1998) for the majority of cases (10 of 13) and $^3J_{CO,CO}$ is significant (3–5 Hz) (Hu and Bax 1996). This leads to artifacts in profiles and hence errors in extracted parameters in cases where the $^3J_{CO,CO}$ coupling is not refocused.

The kinetics and thermodynamics of Im7 exchange are sensitive to solution conditions and this has been exploited to further cross-validate the methodology. Asx/Glx side-chain carbonyl dispersion profiles have been recorded (scheme of Fig. 1) on an Im7 sample in 95% $H_2O$/5% $D_2O$ solvent, 10°C, that shifts the populations and rates, ($k_{ex}$, $p_B$) = (309 ± 40 $s^{-1}$, 1.62 ± 0.14%), from values obtained at 25°C, 100% $D_2O$ (see above). Backbone amide dispersions have also been measured and the data fitted to yield ($k_{ex}$, $p_B$) = (314 ± 11 $s^{-1}$, 1.59 ± 0.04%), in excellent agreement with the side-chain data. Figure 5c compares side-chain carbonyl $|\Delta\varpi|$ values for Asx/Glx residues obtained from fits of dispersions recorded in $D_2O$, pH 6.6, 25°C (*Y*-axis) and 95% $H_2O$/5% $D_2O$, pH 6.6, 10°C (*X*-axis). A strong correlation is obtained and the slight differences (RMSD = 0.12 ppm) are in keeping with what has been noted when $^{15}N$ or $^1H^N$ $|\Delta\varpi|$ values obtained from data measured at different temperatures and/or pH values are compared. As a final test of the robustness of the

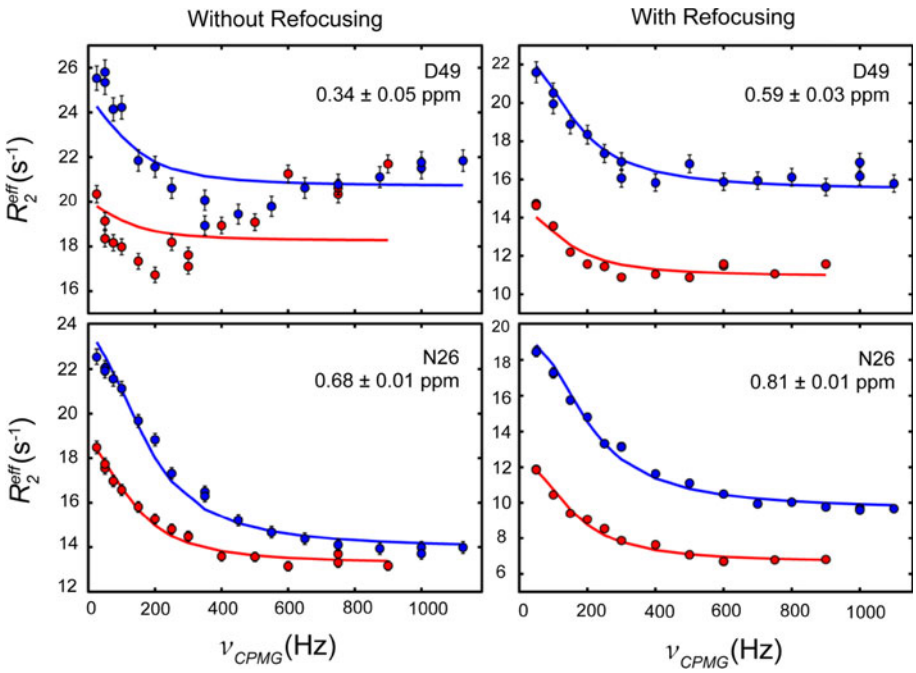


**Fig. 4** Comparison of Asx side-chain CO CPMG relaxation dispersion profiles recorded on Im7 (25°C, pH 6.6, $D_2O$) without (*left*) and with (*right*) the $J_{CO,CO}$ refocusing element. *Solid lines* are best-fits of data recorded at 11.7 (*red*) and 18.8 (*blue*) *T* to a global, two-site exchange model. *Insets* indicate the fitted $|\Delta\varpi|$ value for each residue. The $C^{\gamma}$—backbone CO torsion angles for Asn 26 and Asp 49 are trans (165° and 155°, respectively) (Chak et al. 1996; Dennis et al. 1998), leading to large 3-bond scalar couplings $J_{CO,CO}$ (Hu and Bax 1996) and hence substantial artifacts in dispersion profiles recorded without the refocusing element (Ishima et al. 2004; Lundstrom et al. 2008)

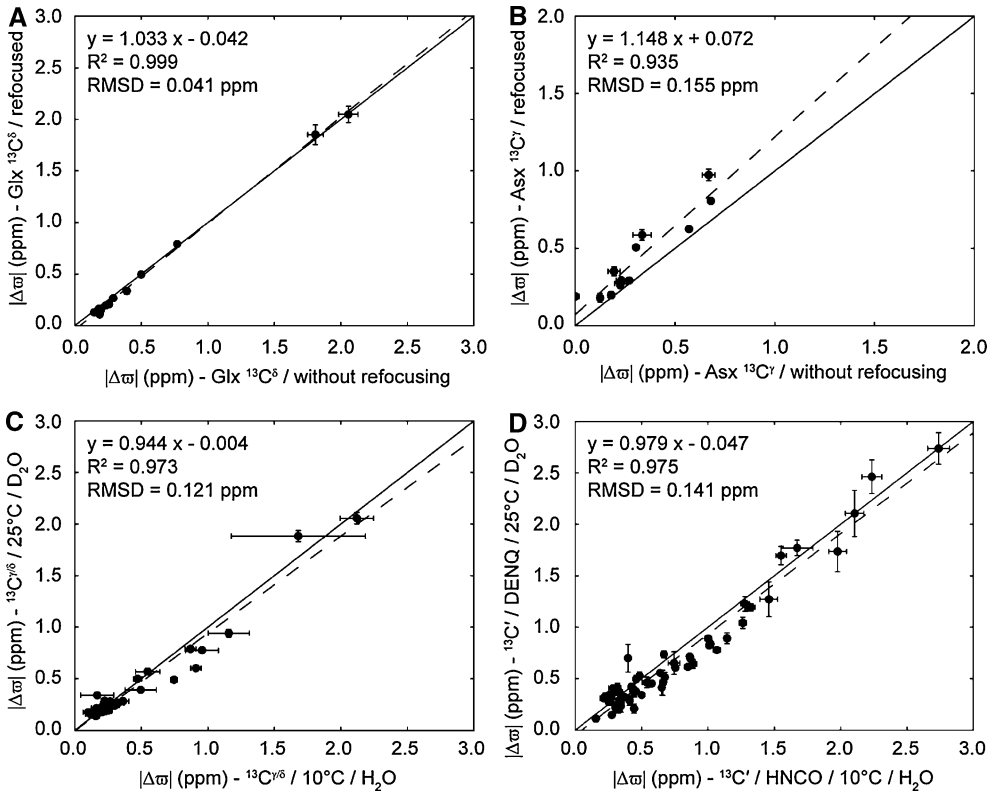


**Fig. 5** Correlations of carbonyl $|\Delta\varpi|$ values extracted from global, two-site exchange fits of CPMG relaxation dispersion profiles recorded on Im7 under a variety of different conditions. *Solid lines* correspond to $y = x$ while *dashed lines* are best-fit linear correlations (*upper left* of each plot). Linear correlations of side-chain carbonyl $|\Delta\varpi|$ values extracted from data recorded with (*Y*-axis) and without (*X*-axis) the $J_{CO,CO}$ refocusing element are shown for Glx (**a**) and Asx (**b**) residues. **c** Correlation of side-chain CO chemical shift differences from dispersion data sets recorded in $D_2O$ at 25°C (*Y*-axis) and 95% $H_2O$/5% $D_2O$ at 10°C (*X*-axis). **d** Comparison of backbone CO $|\Delta\varpi|$ values recorded using the pulse scheme of Fig. 1 (*Y*-axis) and an HNCO-based sequence (*X*-axis) (Lundstrom et al. 2008)

methodology we have correlated backbone carbonyl shift differences extracted from the scheme of Fig. 1 (25°C, $D_2O$, pH 6.6) with those obtained from a previously published HNCO-based experiment (Lundstrom et al. 2008) recorded at 10°C, using 95% $H_2O$/5% $D_2O$ solvent, pH 6.6 and a very high level of agreement is obtained. It is noteworthy that the RMSD between $|\Delta\varpi|$ values measured by the two different approaches is close to a factor of 7 better than the accuracy of carbonyl chemical shift predictions from structure using state of the art programs (Shen and Bax 2010).

In Fig. 6 the $|\Delta\varpi|$ values obtained for the 26 side-chain carbonyl groups of Im7 are color coded on the crystal structure of Im7 (Dennis et al. 1998). As expected, the largest chemical shift changes occur proximal to helix 3 which is known to be unfolded in the folding intermediate (Gorski et al. 2004). In addition, large shift differences are noted for Glu 25 and Asn 26 at the C-terminal end of helix 1. A hydrogen bond is observed between Asn 26 and Tyr 55 in helix 3 in the ground state crystal structure, so that the large $|\Delta\varpi|$ for Asn 26 suggests that this interaction is weakened or eliminated in the excited state. Signs for ten $\Delta\varpi$ values above 0.35 ppm could be confidently obtained by comparing carbonyl resonance positions at 11.7 and 18.8 T (Skrynnikov et al. 2002). For eight of the ten values $\varpi_E$ is closer to the random coil value (Glu ~183.5 ppm, Asp ~180.0 ppm, Gln ~180.0 ppm, Asn ~177.0 ppm) (Tollinger et al. 2005; Ulrich et al. 2008) than $\varpi_G$, consistent with an excited state conformation that is more 'unfolded' than in the ground state. Interestingly, Asn 79, one of the two residues that shifts away from random coil in the excited state, has chemical shifts clearly influenced by the proximal Trp 75 (see Fig. 2), suggesting that the relative orientation of the carbonyl group with respect to the Trp ring changes between ground and excited conformations.

Helix 1 of the ground state is stabilized in part by two internal salt-bridges, Glu 21-Lys 24 and Glu 23-Lys 20 (Dennis et al. 1998). Notably, a small $|\Delta\varpi|$ value is obtained for Glu 23 (0.24 ± 0.01 ppm) while side-chain CO groups for Glu 21 and the helix-capping residue Glu 25 move to random coil positions in the excited state. These observations are consistent with an intact Glu 23-Lys 20 salt-bridge in the excited state, with helix 1 shortened by a residue or two. Indeed, backbone chemical shifts obtained from CPMG experiments (data not shown) indicate a much more dynamic loop connecting helices 1 and 2 and a shorter helix 1. In a similar manner, the small $|\Delta\varpi|$ for Glu

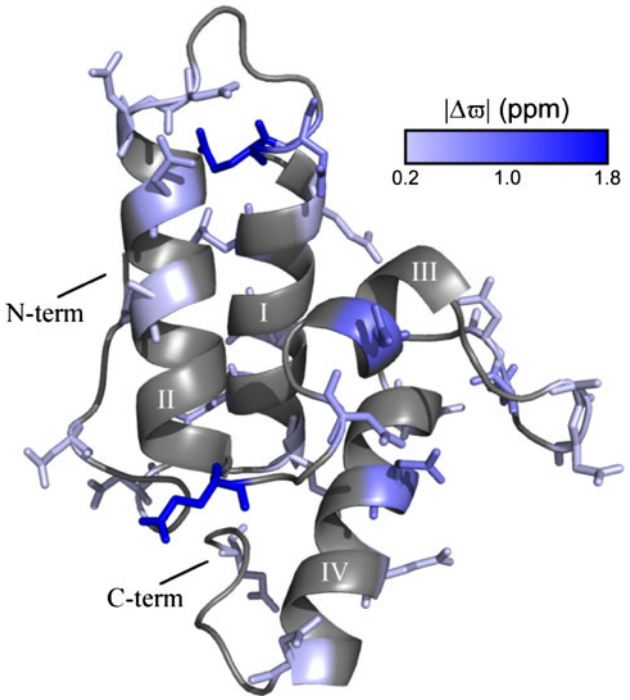


**Fig. 6** Distribution of $|\Delta\varpi|$ values obtained for side-chain carbonyl groups (indicated using a *stick* representation) of Im7 color coded on a ribbon diagram of the Im7 structure, PDB ID: 1AYI (Dennis et al. 1998). The *four helices* in the structure are labeled with roman numerals

12 ($0.28 \pm 0.01$ ppm) may indicate that a native salt-bridge between Glu 12 and Lys 73 linking helix 1 and helix 4 in the ground state is still present in the intermediate state, either in part or in full. Overall, the side-chain data presented here indicate an excited conformer that is more unfolded-like than the ground state, albeit with a number of crucial native interactions in place.

In addition to reporting on differences in salt bridge or hydrogen bonding interactions, changes in side-chain $^{13}$CO $|\Delta\varpi|$ values may also reflect differences in carboxyl pKa's between exchanging states. In principle, pKa values of carboxylic groups in the excited state can be measured by performing a pH dependent relaxation dispersion study so that $\varpi_E$ versus pH can be obtained. In practice, this requires a system for which both high quality spectra and significant dispersions are present over a broad pH range. This is unfortunately not the case for the Im7 protein considered here where spectra become excessively broadened below pH 6.0 and where the excited state population decreases rather significantly for pH values about approximately 7.

In summary, we have presented a new pulse scheme for the measurement of side-chain carbonyl CPMG relaxation dispersion profiles in U-[$^{13}$C]-labeled proteins. The experiment complements existing methodology that probes millisecond time-scale dynamics at methyl group (Lundstrom et al. 2007; Skrynnikov et al. 2001), $C^{\beta}$ (Lundstrom and Kay 2009), Asn/Gln $NH_2$ (Mulder et al. 2001) and Lys $NH_3^+$ (Esadze et al.) side-chain positions. Combined with backbone chemical shifts and orientational restraints measured using similar CPMG-based approaches, this information will be extremely valuable in obtaining quantitative structural descriptions of low populated protein conformations.

**Acknowledgments** The authors thank Dr. Sara Whittaker and Professors Geoff Moore and Sheena Radford for the gift of Im7 constructs. A.L.H. acknowledges the National Science Foundation for post-doctoral support (OISE-0852964). This work was supported by grants from the Canadian Institutes of Health Research and the Natural Sciences and Engineering Research Council of Canada (LEK). L.E.K. holds a Canada Research Chair in Biochemistry.

## References

Auer R, Neudecker P, Muhandiram DR, Lundstrom P, Hansen DF, Konrat R, Kay LE (2009) Measuring the signs of 1H(alpha) chemical shift differences between ground and excited protein states by off-resonance spin-lock R(1rho) NMR spectroscopy. J Am Chem Soc 131:10832–10833

Baldwin AJ, Kay LE (2009) NMR spectroscopy brings invisible protein states into focus. Nat Chem Biol 5:808–814

Boehr DD, McElheny D, Dyson HJ, Wright PE (2006) The dynamic energy landscape of dihydrofolate reductase catalysis. Science 313:1638–1642

Bouvignies G, Korzhnev DM, Neudecker P, Hansen DF, Cordes MH, Kay LE (2010) A simple method for measuring signs of (1)H(N) chemical shift differences between ground and excited protein states. J Biomol NMR 47:135–141

Capaldi AP, Shastry MC, Kleanthous C, Roder H, Radford SE (2001) Ultrarapid mixing experiments reveal that Im7 folds via an on-pathway intermediate. Nat Struct Biol 8:68–72

Capaldi AP, Kleanthous C, Radford SE (2002) Im7 folding mechanism: misfolding on a path to the native state. Nat Struct Biol 9:209–216

Cavalli A, Salvatella X, Dobson CM, Vendruscolo M (2007) Protein structure determination from NMR chemical shifts. Proc Natl Acad Sci USA 104:9615–9620

Chak KF, Safo MK, Ku WY, Hsieh SY, Yuan HS (1996) The crystal structure of the immunity protein of colicin E7 suggests a possible colicin-interacting surface. Proc Natl Acad Sci USA 93:6437–6442

Delaglio F, Grzesiek S, Vuister GW, Zhu G, Pfeifer J, Bax A (1995) NMRPipe: a multidimensional spectral processing system based on UNIX pipes. J Biomol NMR 6:277–293

Dennis CA, Videler H, Pauptit RA, Wallis R, James R, Moore GR, Kleanthous C (1998) A structural comparison of the colicin immunity proteins Im7 and Im9 gives new insights into the molecular determinants of immunity-protein specificity. Biochem J 333(Pt 1):183–191

Esadze A, Li DW, Wang T, Bruschweiler R, Iwahara J (2011) Dynamics of lysine side-chain amino groups in a protein studied by heteronuclear 1H–15 N NMR spectroscopy. J Am Chem Soc 133:909–919

Fraser JS, Clarkson MW, Degnan SC, Erion R, Kern D, Alber T (2009) Hidden alternative structures of proline isomerase essential for catalysis. Nature 462:669–673

Geen H, Freeman R (1991) Band-selective radiofrequency pulses. J Magn Reson 93:93–141

Gerstein M (1997) A structural census of genomes: comparing bacterial, eukaryotic, and archaeal genomes in terms of protein structure. J Mol Biol 274:562–576

Goddard TD, Kneller D SPARKY 3. University of California, San Francisco

Gorski SA, Le Duff CS, Capaldi AP, Kalverda AP, Beddard GS, Moore GR, Radford SE (2004) Equilibrium hydrogen exchange reveals extensive hydrogen bonded secondary structure in the on-pathway intermediate of Im7. J Mol Biol 337:183–193

Hansen DF, Vallurupalli P, Kay LE (2008a) An improved 15 N relaxation dispersion experiment for the measurement of millisecond time-scale dynamics in proteins. J Phys Chem 112:5898–5904

Hansen DF, Vallurupalli P, Kay LE (2008b) Using relaxation dispersion NMR spectroscopy to determine structures of excited, invisible protein states. J Biomol NMR 41:113–120

Hansen DF, Vallurupalli P, Lundstrom P, Neudecker P, Kay LE (2008c) Probing chemical shifts of invisible states of proteins with relaxation dispersion NMR spectroscopy: how well can we do? J Am Chem Soc 130:2667–2675

Hu JS, Bax A (1996) Measurement of three-bond 13C–13C J couplings between carbonyl and carbonyl/carboxyl carbons in isotopically enriched proteins. J Am Chem Soc 118:8170–8171

Ishima R, Torchia DA (1999) Estimating the time scale of chemical exchange of proteins from measurements of transverse relaxation rates in solution. J Biomol NMR 14:369–372

Ishima R, Torchia D (2003) Extending the range of amide proton relaxation dispersion experiments in proteins using a constant-time relaxation-compensated CPMG approach. J Biomol NMR 25:243–248

Ishima R, Baber J, Louis JM, Torchia DA (2004) Carbonyl carbon transverse relaxation dispersion measurements and ms-micros timescale motion in a protein hydrogen bond network. J Biomol NMR 29:187–198

Karplus M, Kuriyan J (2005) Molecular dynamics and protein function. Proc Natl Acad Sci USA 102:6679–6685

Kay LE (1993) Pulsed-field gradient-enhanced three-dimensional NMR experiment for correlating $^{13}C^{a}/^{b}$, $^{13}C'$ and $^{1}H^{a}$ chemical shifts in uniformly $^{13}$C-labeled proteins dissolved in $H_2O$. J Am Chem Soc 115:2055–2057

Korzhnev DM, Salvatella X, Vendruscolo M, Di Nardo AA, Davidson AR, Dobson CM, Kay LE (2004) Low-populated folding intermediates of Fyn SH3 characterized by relaxation dispersion NMR. Nature 430:586–590

Korzhnev DM, Religa TL, Banachewicz W, Fersht AR, Kay LE (2010) A transient and low-populated protein-folding intermediate at atomic resolution. Science 329:1312–1316

Kupce E, Freeman R (1996) Optimized adiabatic pulses for wideband inversion. J Magn Reson Ser A 118:299–303

Kupce E, Wagner G (1996) Multisite band-selective decoupling in proteins. J Magn Reson B 110:309–312

Le Duff CS, Whittaker SB, Radford SE, Moore GR (2006) Characterisation of the conformational properties of urea-unfolded Im7: implications for the early stages of protein folding. J Mol Biol 364:824–835

Loria JP, Rance M, Palmer AG (1999) A relaxation compensated CPMG sequence for characterizing chemical exchange. J Am Chem Soc 121:2331–2332

Lundstrom P, Kay LE (2009) Measuring 13Cb chemical shifts of invisible excited states in proteins by relaxation dispersion NMR spectroscopy. J Biomol NMR 44:139–155

Lundstrom P, Vallurupalli P, Religa TL, Dahlquist FW, Kay LE (2007) A single-quantum methyl 13C-relaxation dispersion experiment with improved sensitivity. J Biomol NMR 38:79–88

Lundstrom P, Hansen DF, Kay LE (2008) Measurement of carbonyl chemical shifts of excited protein states by relaxation dispersion NMR spectroscopy: comparison between uniformly and selectively (13)C labeled samples. J Biomol NMR 42:35–47

Lundstrom P, Hansen DF, Vallurupalli P, Kay LE (2009) Accurate measurement of alpha proton chemical shifts of excited protein states by relaxation dispersion NMR spectroscopy. J Am Chem Soc 131:1915–1926

Marion D, Ikura M, Tschudin R, Bax A (1989) Rapid recording of 2D NMR spectra without phase cycling. Application to the study of hydrogen exchange in proteins. J Magn Reson 85:393–399

Millet O, Loria JP, Kroenke CD, Pons M, Palmer AG (2000) The static magnetic field dependence of chemical exchange linebroadening defines the NMR chemcial shift time scale. J Am Chem Soc 122:2867–2877

Mulder FA, Akke M (2003) Carbonyl 13C transverse relaxation measurements to sample protein backbone dynamics. Magn Reson Chem 41:853–865

Mulder FAA, Skrynnikov NR, Hon B, Dahlquist FW, Kay LE (2001) Measurement of slow timescale dynamics in protein sidechains by 15 N relaxation dispersion NMR spectroscopy: Application to Asn and Gln residues in a cavity mutant of T4 lysozyme. J Am Chem Soc 123:967–975

Orekhov VY, Korzhnev DM, Kay LE (2004) Double- and zero-quantum NMR relaxation dispersion experiments sampling millisecond time scale dynamics in proteins. J Am Chem Soc 126:1886–1891

Palmer AG, Kroenke CD, Loria JP (2001) NMR methods for quantifying microsecond-to-millisecond motions in biological macromolecules. Methods Enzym 339:204–238

Press WH, Flannery BP, Teukolsky SA, Vetterling WT (1988) Numerical recipes in C. Cambridge University Press, Cambridge

Shen Y, Bax A (2010) SPARTA + : a modest improvement in empirical NMR chemical shift prediction by means of an artificial neural network. J Biomol NMR 48:13–22

Shen Y, Delaglio F, Cornilescu G, Bax A (2009) TALOS +: a hybrid method for predicting protein backbone torsion angles from NMR chemical shifts. J Biomol NMR 44:213–223

Skrynnikov NR, Mulder FAA, Hon B, Dahlquist FW, Kay LE (2001) Probing slow time scale dynamics at methyl-containing side chains in proteins by relaxation dispersion NMR measurements: Application to methionine residues in a cavity mutant of T4 lysozyme. J Am Chem Soc 123:4556–4566

Skrynnikov NR, Dahlquist FW, Kay LE (2002) Reconstructing NMR spectra of "invisible" excited protein states using HSQC and HMQC experiments. J Am Chem Soc 124:12352–12360

Tollinger M, Skrynnikov NR, Mulder FAA, Forman-Kay JD, Kay LE (2001) Slow dynamics in folded and unfolded states of an SH3 domain. J Am Chem Soc 123:11341–11352

Tollinger M, Kay LE, Forman-Kay JD (2005) Measuring pK(a) values in protein folding transition state ensembles by NMR spectroscopy. J Am Chem Soc 127:8904–8905

Ulrich EL, Akutsu H, Doreleijers JF, Harano Y, Ioannidis YE, Lin J, Livny M, Mading S, Maziuk D, Miller Z, Nakatani E, Schulte CF, Tolmie DE, Wenger RK, Yao H, Markley JL (2008) BioMagResBank. Nucleic Acids Res 36: D402–D408

Vallurupalli P, Hansen DF, Stollar EJ, Meirovitch E, Kay LE (2007) Measurement of bond vector orientations in invisible excited states of proteins. Proc Natl Acad Sci USA 104:18473–18477

Vuister GW, Bax A (1992) Resolution enhancement and spectral editing of uniformly $^{13}$C-enriched proteins by homonuclear broadband $^{13}$C decoupling. J Magn Reson 98:428–435

Whittaker SB, Spence GR, Grossmann JG, Radford SE, Moore GR (2007) NMR analysis of the conformational properties of the trapped on-pathway folding intermediate of the bacterial immunity protein Im7. J Mol Biol 366:1001–1015

Wishart DS, Arndt D, Berjanskii M, Tang P, Zhou J, Lin G (2008) CS23D: a web server for rapid protein structure generation using NMR chemical shifts and sequence data. Nucleic Acids Res 36: W496–W502